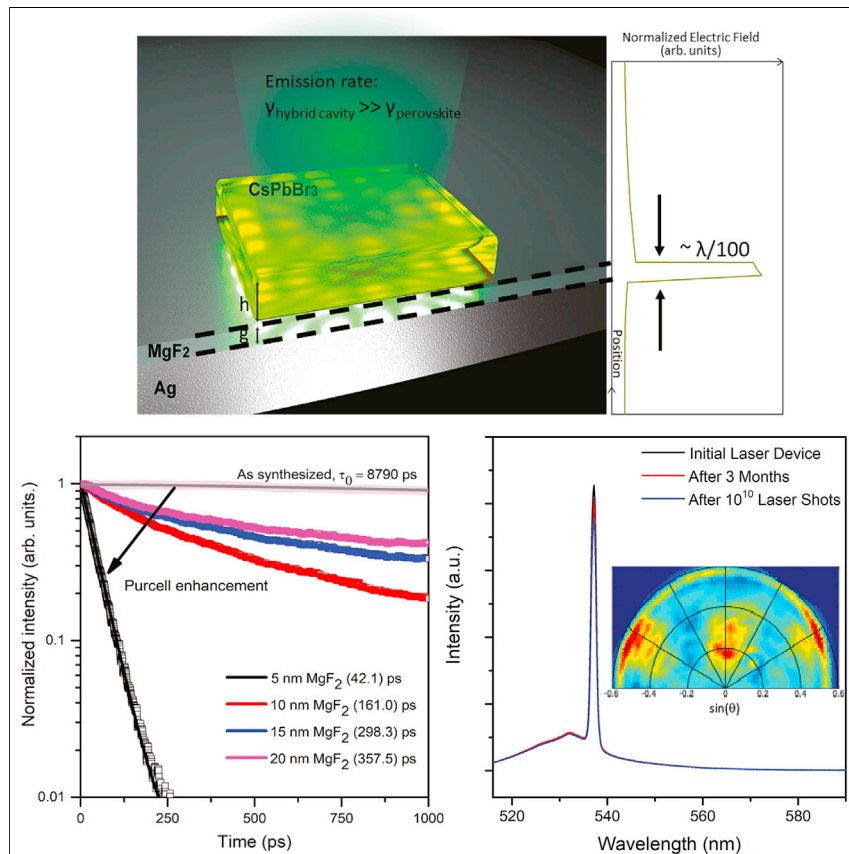


## Article

## Subwavelength-scale lasing perovskite with ultrahigh Purcell enhancement



The capability to control light-matter interfaces creates enormous opportunities across a wide spectrum of photophysical applications. This work demonstrates giant Purcell enhancement in a subwavelength perovskite lasing cavity leading to unparalleled spatiotemporal control with tailored ultrafast emission dynamics and radiation patterns. The well-devised subdiffractive mode confinement residing outside the perovskite region greatly enhances the long-term reliability and operational stability of the perovskite-based devices, show prospective robust applications in ultrafast integrated photonics and optoelectronics.

**Demonstrate**

Proof-of-concept of performance with intended application/response

4

Sui Yang, Wei Bao, Xiaoze Liu, ..., Renmin Ma, Yuan Wang, Xiang Zhang

xiang@berkeley.edu

**Highlights**

Ultrahigh Purcell enhancement is achieved in perovskite-based nanolaser devices

Intrinsically slow emission characteristics of perovskites has been overcome

Subdiffractive single-mode lasing has predefined spatiotemporal characteristics

Enhanced perovskite-based device stability is achieved by migrated mode confinement

## Article

# Subwavelength-scale lasing perovskite with ultrahigh Purcell enhancement

Sui Yang,<sup>1,2,6</sup> Wei Bao,<sup>1,6</sup> Xiaoze Liu,<sup>1,6</sup> Jeongmin Kim,<sup>1</sup> Rongkuo Zhao,<sup>1</sup> Renmin Ma,<sup>4,5</sup> Yuan Wang,<sup>1</sup> and Xiang Zhang<sup>1,3,7,\*</sup>

## SUMMARY

The remarkable photophysical properties of halide perovskites have led to high-performance lasers. The slow emission dynamics and diffraction-limited device, however, impose an intrinsic barrier on realizing ultrafast and compact lasers for integrated optoelectronic applications. Plasmonic cavities have been employed to reduce laser size. Yet the emission dynamics is fundamentally limited due to the dilemma between ever-reduced cavity size and the increase of losses. Here, we show a subwavelength-scale lasing perovskite with ultrahigh Purcell enhancement of 209 that greatly enhances emission dynamics under ambient conditions. The hybrid surface plasmon polaritons (SPPs) coupled with perovskites significantly reduce plasmonic and trap state loss channels and promote a strong Purcell effect. Moreover, the realization of SPPs confinement away from the perovskite region mitigates gain degradations that enables superior long-term device stability and reliability. Our study opens a new avenue for on-chip ultrafast optoelectronics and fundamental studies of light-matter interactions at the strongly confined field.

## INTRODUCTION

Metal halide perovskites  $\text{ABX}_3$  (where A is organic/inorganic cation, B is commonly  $\text{Pb}^{2+}$ , and X is a halide) emerged recently as excellent candidates for third-generation solar cells and solid-state lighting materials.<sup>1,2</sup> In contrast to conventional semiconductors, perovskites exhibit many remarkable properties, including large absorption coefficient ( $\sim 10^4 \text{ cm}^{-1}$  near the band edge),<sup>3</sup> high charge-carrier mobility (exceeding  $10 \text{ cm}^2 \text{ V}^{-1} \text{ s}^{-1}$ ),<sup>4</sup> long carrier lifetime ( $\sim 10^{1-2} \text{ ns}$ ) and diffusion length ( $> 1 \mu\text{m}$ ),<sup>5,6</sup> and high quantum yield, as well as low defect and trap densities<sup>7-9</sup> due to their ionic bond nature. On a par with the rapid advances of photovoltaics, these outstanding attributes also make halide perovskites excellent lasing materials for prospective future optoelectronics.<sup>9-17</sup>

Strategies to construct ultra-compact and fast nanolasers hold the key promise for future optoelectronics, ranging from next-generation optical communications to implantable computing microchips. A plausible solution to such nanolasers is based on surface plasmon amplification by stimulated emission of radiation that can decouple the wavelength scale from free space, and therefore pave the way to a new class of small lasing devices.<sup>18-21</sup> The plasmonic laser device has been demonstrated in recent years by utilizing the remarkable photophysical properties of perovskites.<sup>22-24</sup> However, the slow exciton recombination due to long carrier lifetime in perovskites impose a fundamental limit to laser emission dynamics.

## Progress and potential

Achieving tailored photophysical properties of matter for important device applications is of broad and growing significance. The ionic semiconductors, halide perovskites, emerge as an outstanding light source for their remarkable photophysical properties. However, their intrinsic long carrier lifetime and diffraction-limited device dimensions impose a fundamental barrier on realizing ultrafast on-chip integrated optoelectronic applications. In this work, we report subwavelength-scale perovskite lasing with ultrahigh Purcell enhancement, which overcomes the intrinsically slow emission characteristics of perovskite-based devices. The ultrafast single-mode lasing action has been unveiled under ambient conditions. Meanwhile, the realization of electromagnetic confinement outside the perovskite region mitigates gain degradations, which enables superior long-term device stability. Our demonstration presents a unique and reliable platform for ultrafast integrated photonics and optoelectronics.

The Purcell enhancement, which enhances spontaneous emission rate and scales inversely with the cavity mode volume, receives growing significance in the pursuit of controlled and tailored light-matter interfaces. Furthermore, owing to the intrinsic proportional relationship between Einstein's A (spontaneous) and B (stimulated) coefficients, the Purcell effect can enhance both spontaneous and stimulated emission rate.<sup>25</sup> For a laser system with gain media coupled to an electromagnetic cavity, the tailored spontaneous and stimulated emission rate can be expressed by:<sup>25,26</sup>

$$R_{\text{cav}} = \frac{2Q_{\text{eff}}}{\hbar\epsilon_0\epsilon_a V_{\text{eff}}} d_{ij}^2 (N_{\text{ph}} + 1), \quad (\text{Equation 1})$$

where  $\epsilon_0$  and  $\epsilon_a$  are the dielectric permittivity in the free space and the active material, respectively;  $d_{ij}$  is the dipole matrix element of emitter;  $Q_{\text{eff}}$  and  $V_{\text{eff}}$  represent the effective quality factor and effective mode volume of the cavity mode;  $N_{\text{ph}}$  is the number of photons in the mode ( $N_{\text{ph}} = 0$  considered for the case of spontaneous emission). Thus, a strong Purcell effect (high Purcell enhancement) requires highly efficient coupling between both emitters and cavities, demanding a list of requirements, such as large ratio of  $Q_{\text{eff}}/V_{\text{eff}}$ , reduced loss channels, and high directionality of emission patterns.

Yet by simply reducing the cavity size coupled with surface plasmon, it not only suffers from intrinsic losses in the metal, but also is compromised by the dissipation of confined energy at the ever-reduced mode size. Eventually, by further reducing mode volume of the plasmonic laser to promote Purcell enhancement, the cavity usually cannot maintain enough gain for optical amplification and stimulated emission. Achieving high Purcell enhancement with sustained gain for stimulated emission or lasing is still challenging in the field. For these reasons, only a modest Purcell enhancement factor (typically at the order of tens) for all lasing nanocavities has been experimentally observed so far. As a result, the limited Purcell enhancement fundamentally impedes the operation speed and efficiency of nanolasers.<sup>25,27,28</sup>

## RESULTS AND DISCUSSION

We report ultrahigh Purcell enhancement at room temperature enabled in a hybrid plasmonic nanocavity by coupling ionic perovskite semiconductor with an ultra-smooth silver (Ag) film (roughness < 1 nm) (Figures 1 and S1). The nanolasing cavity integrates a thin perovskite crystal with a metallic surface (Ag) in close proximity separated by a MgF<sub>2</sub> dielectric gap  $g = 5$  nm (Figures 1A and 1B). By hybridizing perovskite emission photons with the surface plasmon of Ag, the emission characteristics can decouple the wavelength scale from free space in a highly confined subwavelength space. That is, the emitted photon from gain medium (CsPbBr<sub>3</sub>) hybridizes with the surface plasmon of Ag, which stores electromagnetic energy in the gap region (< $\lambda/100$ ). Such hybrid SPPs confine the electromagnetic energy in a subwavelength dielectric gap region, which not only leads to an effective optical confinement but also reduces the metal losses simultaneously. Moreover, the achieved ultra-smooth Ag film significantly reduces the scattering loss channels. The thickness of perovskite ( $h$ ) and the size of gap ( $g$ ) are chosen to optimize the gain overlap and to avoid any quenching effect that causes losses of optical energy.<sup>29,30</sup> With well-controlled perovskite nanocrystal geometry and thickness, only transverse magnetic (TM) mode will be coupled and strongly confined in the gap (Figures S2 and S3). Cesium lead bromide (CsPbBr<sub>3</sub>) is selected as lasing gain material due to its superior chemical stability and highly efficient and robust photoluminescence (PL) in the perovskite family.<sup>31–33</sup> With a surfactant-free synthesis (clean surface) technique

<sup>1</sup>Nano-scale Science and Engineering Center (NSEC), University of California at Berkeley, 3112 Etcheverry Hall, Berkeley, CA 94720, USA

<sup>2</sup>Materials Science and Engineering, School for Engineering of Matter Transport and Energy, Arizona State University, Tempe, AZ 85287, USA

<sup>3</sup>Faculty of Science and Faculty of Engineering, The University of Hong Kong, Hong Kong, China

<sup>4</sup>State Key Lab for Mesoscopic Physics and School of Physics, Peking University, Beijing 100871, China

<sup>5</sup>Collaborative Innovation Center of Quantum Matter, Beijing 100871, China

<sup>6</sup>These authors contributed equally

<sup>7</sup>Lead contact

\*Correspondence: [xiang@berkeley.edu](mailto:xiang@berkeley.edu)

<https://doi.org/10.1016/j.matt.2021.10.024>

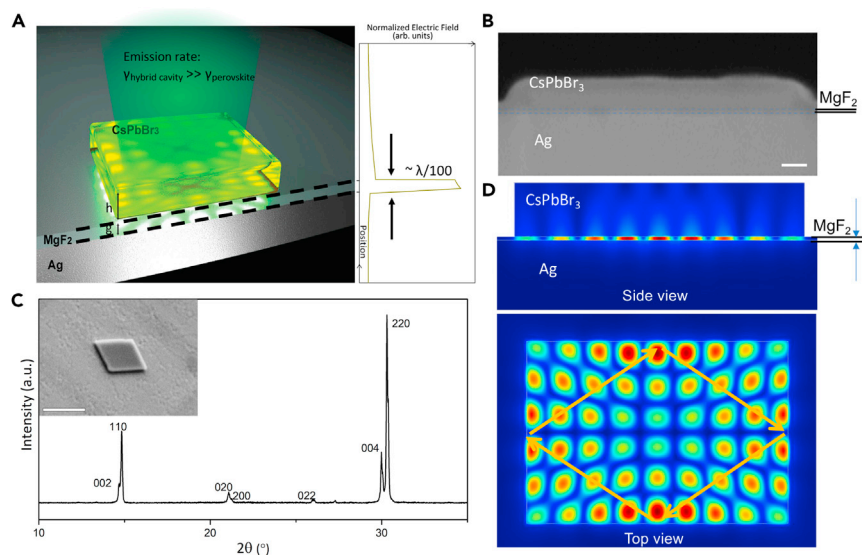


**Figure 1. Schematic of accelerating emission dynamics (Purcell effect) by subwavelength perovskite lasing nanocavity with a highly confined optical mode ( $g < \lambda/100$ ) hybridizing with surface plasmons**

(A) A CsPbBr<sub>3</sub> nanoplate (thickness of  $h$ ) sits on top of a silver substrate bridged by a thin MgF<sub>2</sub> film where optical energy builds up (normalized electric field distribution, right panel). Due to the strong optical confinement, the emission rate of the hybrid plasmon-perovskite cavity is much faster than that of perovskite CsPbBr<sub>3</sub>.

(B) Cross-sectional SEM image of the laser device shows the “sandwiched” laser configuration. Scale bar, 50 nm.

(C) The X-ray diffraction pattern confirms the high crystallinity of the synthesized cesium lead bromide CsPbBr<sub>3</sub> nanoplate. Clear splitting of (002)/(110) and (004)/(220) peaks indicates an orthorhombic crystal structure of CsPbBr<sub>3</sub>.<sup>15</sup> Scanning electron microscope (SEM) image of a typical perovskite nanolaser (inset). Scale bar, 1  $\mu$ m (inset).

(D) Three-dimensional calculation of optical field (norm of electric field) clearly confirms the optical confinement at the gap region (side view). The high intensity resides at each side of the nanoplate indicating total internal reflection (orange arrows) of hybrid SPPs (top view).

(see [experimental procedures](#)), the CsPbBr<sub>3</sub> we synthesized represents well-indexed diffraction peaks and a well-controlled nanocrystal geometry ([Figure 1C](#)). Meanwhile, the total internal reflection of hybrid SPPs forms strong cavity feedback ([Figure 1D](#)), significantly mitigating the radiation loss. Other than enhancing the light-matter interaction with a larger group index for perovskite lasing,<sup>34</sup> all of these factors, by minimizing mode volume via strong confinement, low materials trap state density, and cavity-scattering losses, are the keys to a high-quality nanolasing, promoting strong Purcell enhancement.

[Figure 2A](#) shows how the SPPs-perovskite hybridized feedback of the cavity field promotes, in general, a significant enhancement of photon emission dynamics. Although the spontaneous emission lifetime of perovskite CsPbBr<sub>3</sub> nanoplates is as long as  $\sim 8.79 \pm 0.20$  ns, our configuration significantly promotes free carriers of the perovskite to radiatively recombine much faster than that in the free space. This leads to a drastically accelerated emission dynamics as measured at different gap thickness ([Figure 2A](#)). It can be clearly seen that the emission lifetimes of perovskites decrease significantly as gap size scales down ([Figure 2B](#)). This is due to the increased electromagnetic coupling and confinement at reduced gap size ([Figure S4](#)). Yet further decreasing the gap size to the hot carrier tunneling regime (<5 nm) will result in undemanding quenching effects.<sup>29,30</sup>

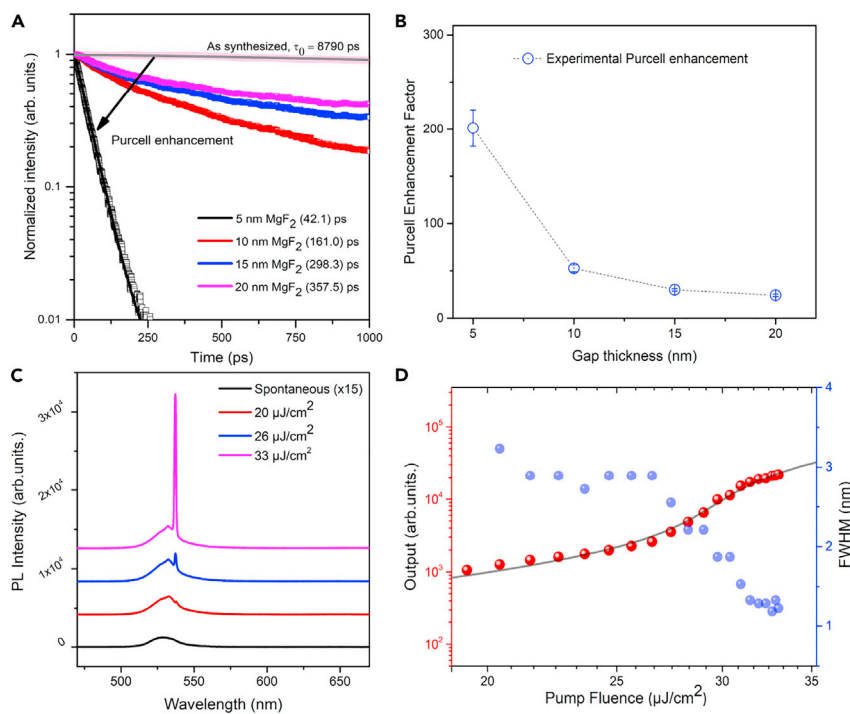


**Figure 2. Purcell enhancement and temporal emission characteristics for nanolasing**

(A) Emission lifetime ( $\tau$ ) measurement as a function of dielectric gap thickness.  $\tau_0$  is emission lifetime in free space. One significant figure after the decimal place is evaluated based on the resolution of a streak camera. The pump fluency is well below the transparent region ( $0.2 \mu\text{J}/\text{cm}^2$ ).  
(B) Average Purcell enhancement factor as a function of dielectric gap thickness. The dotted line is for eye guidance and the measurements from different samples are indicated by the error bars. The sample size for the measurement: the length, width, and height of perovskite nanoplates are around  $1,060 \pm 28$ ,  $833 \pm 15$ , and  $77 \pm 7$  nm, respectively.  
(C) Single-mode lasing spectra under different pumping power at ambient temperature, from spontaneous to amplified spontaneous emission to full lasing oscillation. The sample is at a gap thickness of 5 nm.  
(D) Nonlinear "S-shaped" L-L plot (pump intensity dependence of the photoluminescence emission) with curve fitted from the analytical rate equations. The concurrent linewidth-narrowing behavior clearly signifies the lasing action.

By directly comparing the lifetime measurements, our data indicate that the experimental Purcell enhancement factor  $F$  can be achieved up to 209 with controlled gap size, higher than previously reported lasing devices. This well-contrasting dynamics of the perovskite nanolasing cavity in this work highlights the combined benefits of optical confinement in plasmon cavity, and excellent perovskite photophysical properties due to ionic bonds. The enhancement measurement captures the overall behavior of spontaneous emission enhancement. It should be noted that this enhancement is contrasting to the stimulated emission process, where the emission lifetime is even shorter due to the coherent laser action (Figure S5). However, the high Purcell enhancement factor promises to have a large modulation bandwidth, both below and above the threshold. Thus, it opens a fundamental pathway for improving laser modulation speed<sup>27</sup> (supplemental information, discussion section I). Quantified by the radiative quantum efficiency, we can further analyze the Purcell effect (Purcell enhancement factor as large as 390 for the radiative recombination mechanism) in our system with respect to the radiative portion (supplemental information, discussion section I). It should be noted that the enhanced emission dynamics does not come from the increasing non-radiative emission rate and is mainly an effect resulting from the increasing radiative emission

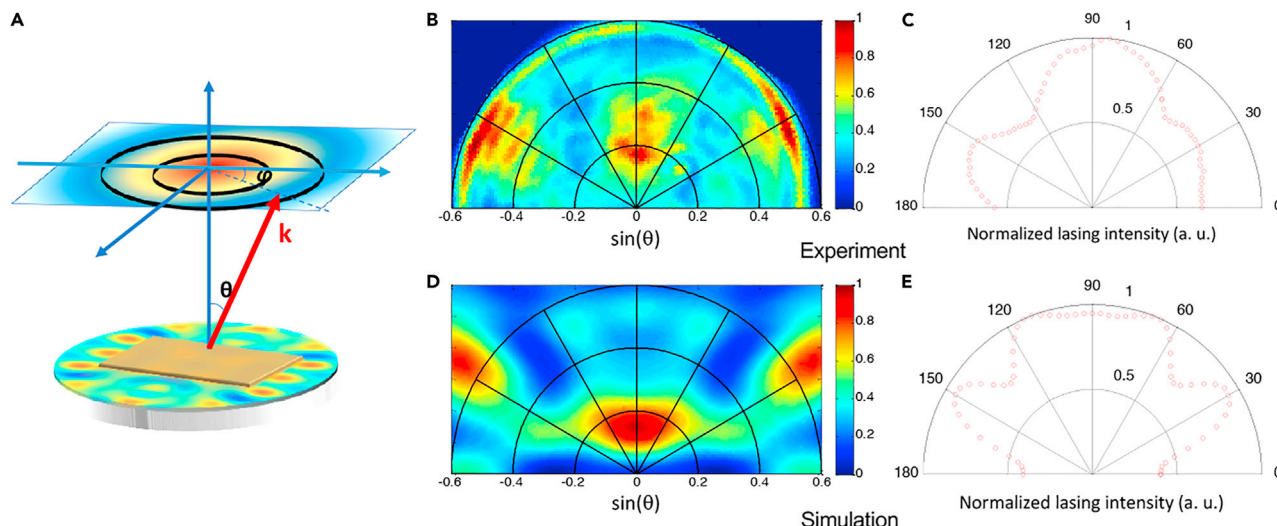


**Figure 3. Spatial emission characteristics**

(A) Schematic of stimulated emission geometry of our device showing coherent emission (simulated Poynting vector, polarization: transverse magnetic [TM]), where the angle  $\theta$  and the angle  $\phi$  represent the polar and azimuthal emission angles, respectively.

(B) The experimental results of far-field  $k$ -space emission patterns of the perovskite-plasmon nanolaser with TM polarization. The polar coordinates refer to the radial coordinates of  $\sin(\theta)$  and the angle coordinates as azimuthal angle  $\phi$ . The well-distributed light intensity signifies highly coherent emission under lasing conditions.

(C) Extracted angular spatial information presents a quantified insight into the lasing property. The angular laser-scattering information reveals the internal cavity feedback scheme with conservation of in-plane SPPs momentum.

(D and E) The corresponding simulation results are presented for comparison in (B) and (C), respectively.

rate, due to the reduced cavity volume. It is well known that halide perovskite materials have long carrier lifetimes and diffusion lengths,<sup>5,6</sup> which enables them high emission efficiency but limits their operation speed. Thus, our result is of particularly high importance for halide perovskite materials in the application of high-speed optoelectronic devices, photonic circuits, and quantum computing.

With such a strong Purcell effect and the outstanding photophysical properties of perovskite in this lasing nanocavity, we, meantime, observed single-mode lasing behavior at ambient temperature even at 5 nm gap confinement. Despite the plasmonic nature, the nanocavity exhibits a low lasing threshold (26  $\mu\text{J}/\text{cm}^2$ ) (Figures 2C and 2D), which is one order of magnitude smaller than that of similar device configurations at ambient temperature and even comparable with the threshold value of the photonic size perovskite laser, with similar shape and chemical compositions.<sup>15,21</sup> With higher pump fluence, the laser device reaches full lasing oscillation with an order of magnitude increase of peak intensity and slightly blue-shifted frequency toward  $\nu_0$  (spontaneous emission frequency) known as the frequency pulling effect.<sup>19</sup> The lasing signature can be clearly seen from the nonlinear kink of the “S-shaped” L-L curve as well as linewidth narrowing (Figure 2D). This clearly shows three photoluminescence regions: spontaneous emission at lower pump power, superlinear increase above transparency regime as an amplified spontaneous emission region, and transition to full laser oscillation.

This large Purcell effect in single-mode lasing action also promotes the high directionality of emission dipoles, which facilitates the stimulated emission as the observed lasing behaviors. The directionality is represented by the spatial distributions of far-field emission patterns. The lasing plasmonic cavity shows well-defined patterns for the strong field confinement along TM polarization, well presented by  $k$ -space (wavevector) PL spectroscopy, as schematically shown in Figure 3A. The angle  $\theta = \arcsin(k_{\parallel}/|k_0|)$  and

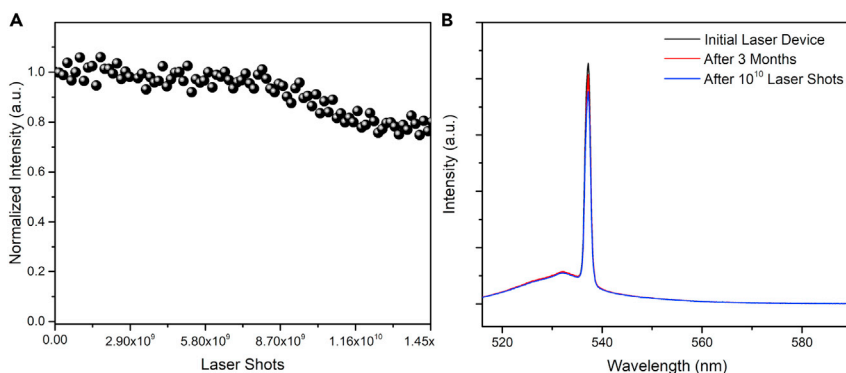


**Figure 4. Stability characterizations of the lasing device**

(A) The testing of the stability of the lasing operations was performed at room temperature and under a pump fluence of  $1.1P_{th}$ ; stable lasing output can sustain  $\sim 10^{10}$  excitation cycles before the intensity falls below 90%.

(B) Device lasing (black) at a gap thickness of 5 nm, tested after exposure at room temperature in air (ambient moisture) for 3 months (red), and after  $1 \times 10^{10}$  laser excitation (thermal) cycles (blue).

$\phi = \text{atan}(k_y/k_x)$  represent the polar and azimuthal emission angles, respectively. The light intensity sustained at certain emissive angle in  $k$ -space (wavevector) PL spectroscopy suggests the highly directional emission of lasing mode (Figure 3B). The signature of emission directionality can be clearly demonstrated at experimentally observed azimuth lobes  $\phi \sim 30^\circ$  and  $150^\circ$ , and  $\sim 75^\circ$  and  $105^\circ$  (Figure 3C). These two symmetric sets of radiation angles result from the mode leaking out at two perpendicular interfaces (i.e., the two lateral sides) of the rectangular-shaped cavity. This observation is in excellent agreement with our three-dimensional far-field radiation simulations (Figures 3D and 3E). The well-contrasted spatial radiative pattern confirms the strong emissive directionality due to the preferred emitting orientations facilitated by strong Purcell effect, prospecting on-chip controllable spatiotemporal optoelectronics.

Furthermore, the fact that the electric field is mostly confined in the MgF<sub>2</sub> gap region in our hybrid perovskite-plasmon lasing devices make them excellent in terms of performance stability, in comparison with previously reported free-standing or other photonic lasers of CsPbBr<sub>3</sub>.<sup>15,35–41</sup> As shown, the preeminently stable lasing output under constant, pulsed excitation above the lasing threshold can sustain over  $\sim 10^{10}$  excitation cycles (Figure 4A). In addition, benefiting from the PDMS polymer residues during the transfer,<sup>42,43,44</sup> the device works almost identically after laser shots and ambient exposure at room temperature for three months (Figure 4B), indicating the excellent long-term operational stability.

## Conclusions

To conclude, we have demonstrated a strong Purcell effect in a perovskite-plasmon coupled lasing nanocavity with dramatically accelerated emission dynamics. The giant Purcell enhancement in the coherent light-based nanosystem enables ultrafast laser dynamics and facilitates laser gain compensation and mode selection. The single-mode lasing action has been observed in the strongly confined laser cavity, which is spatially unveiled with high directionality by a measured  $k$ -space radiation pattern. The work presents a unique platform for applications in integrated optical circuits, single-molecule sensing, ultrafast information processing, and communications. Furthermore, the exceptional photophysical properties of perovskites, combined with novel plasmonic configurations, opens new avenues for optically controlled ultrafast information processing, communications,

and fundamental investigations of light-matter interactions in strongly confined fields.

## EXPERIMENTAL PROCEDURES

### Resource availability

#### Lead contact

Xiang Zhang serves as the lead contact ([xiang@berkeley.edu](mailto:xiang@berkeley.edu)).

#### Materials availability

No new reagents were generated in this study.

#### Data and code availability

All data are available upon reasonable request.

### Materials

Lead(II) iodide  $\text{PbI}_2$  (99.999%), dimethylformamide, cesium bromide  $\text{CsBr}$  (99.999%), methanol, and isopropanol were purchased from Sigma-Aldrich and used without further purification. Single-crystal silicon (100) wafers were from UniversityWafer. Silver and magnesium fluoride  $\text{MgF}_2$  film deposition targets were purchased from the Kurt J. Lesker Company.

### Surfactant-free growth of perovskite nanocrystals

The precursor solution was prepared by  $\text{PbI}_2$  (99.999%) (1 M) in 1 mL anhydrous dimethylformamide and stirred at 70°C to maintain a low supersaturation condition for the crystal growth of perovskites. The substrates were prepared by cutting ~1- × 1-cm glass substrates and washing them sequentially with acetone, isopropanol, and deionized water. Cleaned substrates were then treated with  $\text{O}_2$ -plasma or piranha for 10 min. The precursor solution was spun onto the prepared substrates at 2,000 rpm for 120 s. The substrate was annealed at 100°C for 15 min. The substrate coated with  $\text{PbI}_2$  was carefully placed in cesium bromide  $\text{CsBr}$  (99.999%)/methanol solution (0.04 M) in a glass vial, with the  $\text{PbI}_2$ -coated side facing up to the growth of perovskite nanoplates. The reaction vial was put on a hot plate at 55°C for a reaction time of ~16 h. All chemicals were purchased from Aldrich and used without further purification and all of the synthesis procedure was performed in a glove box. The substrate slide was taken out and subsequently dipped into isopropanol to remove the residual salts. The product was then dried under a stream of  $\text{N}_2$  for further device fabrication.

### Device fabrication

Single-crystal silicon (100) wafer with deep etched marker (35  $\mu\text{m}$  deep) was pre-cleaned by piranha solution, and then coated with 99.99% purity silver using e-beam evaporation (CHA solution) at a pressure of  $<5 \times 10^{-7}$  Torr. The evaporation rate was set to ~10 A/s to avoid oxidation during evaporation. The templated stripped silver film was then prepared by applying a UV curable epoxy (Norland 61A) between the deposited silver surface and a glass chip. After 10 min UV curing, the flat silver film was peeled off from the silicon substrate by gently lifting one edge of the glass chip. Next, 5 nm magnesium fluoride  $\text{MgF}_2$  was evaporated (CHA solution) onto the stripped silver film at a deposition rate of ~0.5 A/s. Finally, the synthetic single-crystal  $\text{CsPbBr}_3$  nanoplates were transferred onto the  $\text{MgF}_2$  film via a PDMS stamp. PDMS residues during the transfer help repel water and maintain the chemical stability of perovskite nanocrystals.<sup>42–44</sup>

### Optical characterization

The lasing characterization and  $k$ -space spatial coherence measurements were carried out in our home-built confocal setup attached with a spectrometer and a 2D

EMCCD array camera (Andor spectrometer). A long working distance objective lens (Nikon Plan Fluor ELWD 40 $\times$ ) was adopted in this work, which has a numerical aperture of 0.6 and objective correction collars for localizing the samples. For the lasing characterization, the wavelength of 470 nm optical parametric oscillator pulse laser (Inspire, Spectra Physics), which is pumped by a mode-locked Ti: sapphire laser (Mai Tai Spectra Physics), was used to pump the samples. The pump power (repetition rate was 80 MHz, pulse duration  $\Delta t = 190$  fs) was tuned in a wide range to monitor the lasing action. The lasing spectra were collected into the Andor spectrometer via the real-space imaging path while the  $k$ -space (far-field) images were obtained via the  $k$ -space imaging path, as shown in Figure S8. For short lifetime measurement, the transient PL signals were collected using a Hamamatsu streak camera (time resolution of 2 ps). For long lifetime measurement, an avalanche photodiode (OEC) with a time resolution of  $\sim$ 100 ps was used in the time-correlated single-photon counting (TCSPC) system.

## SUPPLEMENTAL INFORMATION

Supplemental information can be found online at <https://doi.org/10.1016/j.matt.2021.10.024>.

## ACKNOWLEDGMENTS

This work was supported by the Gordon and Betty Moore Foundation (award no. 5722) and the Ernest S. Kuh Endowed Chair Professorship. S.Y. acknowledges the start-up funding from Arizona State University. The authors acknowledge Quanwei Li for the discussion and support on TCSPC and Jongseo Baek for the assistance on e-beam evaporation.

## AUTHOR CONTRIBUTIONS

S.Y. and X.Z. conceived the project and designed the experiments. S.Y. formulated the theory and fabricated the samples. S.Y., W.B., and X.L. performed the device preparation and measurements with assistance from J.K. R.Z., R.M., and Y.W. contributed to data discussion. S.Y. performed stability measurement. S.Y. and X.Z. wrote the manuscript and all authors contributed to data interpretation and discussion.

## DECLARATION OF INTERESTS

The authors declare no competing interests.

Received: March 10, 2021

Revised: September 29, 2021

Accepted: October 27, 2021

Published: December 1, 2021

## REFERENCES

1. Green, M.A., Ho-Baillie, A., and Snaith, H.J. (2014). The emergence of perovskite solar cells. *Nat. Photon.* **8**, 506–514.
2. Stranks, S.D., and Snaith, H.J. (2015). Metal-halide perovskites for photovoltaic and light-emitting devices. *Nat. Nanotechnol.* **10**, 391–402.
3. De Wolf, S., Holovsky, J., Moon, S.J., Loper, P., Niesen, B., Ledinsky, M., Haug, F.J., Yum, J.H., and Ballif, C. (2014). Organometallic halide perovskites: sharp optical absorption edge and its relation to photovoltaic performance. *J. Phys. Chem. Lett.* **5**, 1035–1039.
4. Leijtens, T., Stranks, S.D., Eperon, G.E., Lindblad, R., Johansson, E.M.J., McPherson, I.J., Rensmo, H., Ball, J.M., Lee, M.M., Snaith, H.J., et al. (2014). Electronic properties of meso-superstructured and planar organometal halide perovskite films: charge trapping, photodoping, and carrier mobility. *ACS Nano* **8**, 7147–7155.
5. Stranks, S.D., Eperon, G.E., Grancini, G., Menelaou, C., Alcocer, M.J.P., Leijtens, T., Herz, L.M., Petrozza, A., and Snaith, H.J. (2013). Electron-hole diffusion lengths exceeding 1 micrometer in an organometal trihalide perovskite absorber. *Science* **342**, 341–344.
6. Zhou, H.P., Chen, Q., Li, G., Luo, S., Song, T.B., Duan, H.S., Hong, Z.R., You, J.B., Liu, Y.S., Yang, Y., et al. (2014). Interface engineering of highly efficient perovskite solar cells. *Science* **345**, 542–546.
7. Stranks, S.D., Burlakov, V.M., Leijtens, T., Ball, J.M., Goriely, A., and Snaith, H.J. (2014).

- Recombination kinetics in organic-inorganic perovskites: excitons, free charge, and subgap states. *Phys. Rev. Appl.* 2, 8.
8. Shi, D., Adinolfi, V., Comin, R., Yuan, M.J., Alarousu, E., Buin, A., Chen, Y., Hoogland, S., Rothenberger, A., Katsiev, K., et al. (2015). Low trap-state density and long carrier diffusion in organolead trihalide perovskite single crystals. *Science* 347, 519–522.
  9. Zhu, H.M., Fu, Y.P., Meng, F., Wu, X.X., Gong, Z.Z., Ding, Q., Gustafsson, M.V., Trinh, M.T., Jin, S., and Zhu, X.Y. (2015). Lead halide perovskite nanowire lasers with low lasing thresholds and high quality factors. *Nat. Mater.* 14, 636–U115.
  10. Deschler, F., Price, M., Pathak, S., Klintberg, L.E., Jarausch, D.D., Higler, R., Hüttnner, S., Leijtens, T., Stranks, S.D., Snaith, H.J., et al. (2014). High photoluminescence efficiency and optically pumped lasing in solution-processed mixed halide perovskite semiconductors. *J. Phys. Chem. Lett.* 5, 1421–1426.
  11. Zhang, Q., Ha, S.T., Liu, X.F., Sum, T.C., and Xiong, Q.H. (2014). Room-temperature near-infrared high-Q perovskite whispering-gallery planar nano lasers. *Nano Lett.* 14, 5995–6001.
  12. Sutherland, B.R., Hoogland, S., Adachi, M.M., Wong, C.T.O., and Sargent, E.H. (2014). Conformal organohalide perovskites enable lasing on spherical resonators. *ACS Nano* 8, 10947–10952.
  13. Yakunin, S., Protesescu, L., Krieg, F., Bodnarchuk, M.I., Nedelcu, G., Humer, M., De Luca, G., Fiebig, M., Heiss, W., and Kovalenko, M.V. (2015). Low-threshold amplified spontaneous emission and lasing from colloidal nanocrystals of caesium lead halide perovskites. *Nat. Commun.* 6, 8.
  14. Sutherland, B.R., and Sargent, E.H. (2016). Perovskite photonic sources. *Nat. Photon.* 10, 295–302.
  15. Eaton, S.W., Lai, M.L., Gibson, N.A., Wong, A.B., Dou, L.T., Ma, J., Wang, L.W., Leone, S.R., and Yang, P.D. (2016). Lasing in robust cesium lead halide perovskite nanowires. *Proc. Natl. Acad. Sci. U S A* 113, 1993–1998.
  16. Fu, Y.P., Zhu, H.M., Stoumpos, C.C., Ding, Q., Wang, J., Kanatzidis, M.G., Zhu, X.Y., and Jin, S. (2016). Broad wavelength tunable robust lasing from single-crystal nanowires of cesium lead halide perovskites ( $\text{CsPbX}_3$ , X = Cl, Br, I). *ACS Nano* 10, 7963–7972.
  17. Zhang, Q., Su, R., Liu, X.F., Xing, J., Sum, T.C., and Xiong, Q.H. (2016). High-quality whispering-gallery-mode lasing from cesium lead halide perovskite nanoplatelets. *Adv. Funct. Mater.* 26, 6238–6245.
  18. Bergman, D.J., and Stockman, M.I. (2003). Surface plasmon amplification by stimulated emission of radiation: quantum generation of coherent surface plasmons in nanosystems. *Phys. Rev. Lett.* 90, 4.
  19. Oulton, R.F., Sorger, V.J., Zentgraf, T., Ma, R.M., Gladden, C., Dai, L., Bartal, G., and

- Zhang, X. (2009). Plasmon lasers at deep subwavelength scale. *Nature* 461, 629–632.
20. Noginov, M.A., Zhu, G., Belgrave, A.M., Bakker, R., Shalaev, V.M., Narimanov, E.E., Stout, S., Herz, E., Suteewong, T., and Wiesner, U. (2009). Demonstration of a spaser-based nanolaser. *Nature* 460, 1110–U1168.
  21. Ma, R.M., Oulton, R.F., Sorger, V.J., Bartal, G., and Zhang, X.A. (2011). Room-temperature sub-diffraction-limited plasmon laser by total internal reflection. *Nat. Mater.* 10, 110–113.
  22. Yu, H.C., Ren, K., Wu, Q., Wang, J., Lin, J., Wang, Z., Xu, J.J., Oulton, R.F., Qu, S.C., and Jin, P. (2016). Organic-inorganic perovskite plasmonic nanowire lasers with a low threshold and a good thermal stability. *Nanoscale* 8, 19536–19540.
  23. Huang, C., Sun, W., Fan, Y., Wang, Y., Gao, Y., Zhang, N., Wang, K., Liu, S., Wang, S., and Xiao, S. (2018). Formation of lead halide perovskite based plasmonic nanolasers and nanolaser arrays by tailoring the substrate. *ACS Nano* 12, 3865–3874.
  24. Li, C., Liu, Z., Shang, Q., and Zhang, Q. (2019). Surface-plasmon-assisted metal halide perovskite small lasers. *Adv. Opt. Mater.* 7, 1900279.
  25. Romeira, B., and Fiore, A. (2018). Purcell effect in the stimulated and spontaneous emission rates of nanoscale semiconductor lasers. *IEEE J. Quan. Electron.* 54, 12.
  26. Auffeves, A., Gerace, D., Gerard, J.M., Santos, M.F., Andreani, L.C., and Poizat, J.P. (2010). Controlling the dynamics of a coupled atom-cavity system by pure dephasing. *Phys. Rev. B* 81, 10.
  27. Bjork, G., and Yamamoto, Y. (1991). Analysis of semiconductor microcavity lasers using rate equations. *IEEE J. Quan. Electron.* 27, 2386–2396.
  28. Altug, H., Englund, D., and Vuckovic, J. (2006). Ultrafast photonic crystal nanocavity laser. *Nat. Phys.* 2, 484–488.
  29. Jin, Y.D., and Gao, X.H. (2009). Plasmonic fluorescent quantum dots. *Nat. Nanotechnol.* 4, 571–576.
  30. Anger, P., Bharadwaj, P., and Novotny, L. (2006). Enhancement and quenching of single-molecule fluorescence. *Phys. Rev. Lett.* 96, 4.
  31. Pan, J., Sarmah, S.P., Murali, B., Dursun, I., Peng, W., Parida, M.R., Liu, J., Sinatra, L., Alyami, N., Zhao, C., et al. (2015). Air-stable surface-passivated perovskite quantum dots for ultra-robust, single- and two-photon-induced amplified spontaneous emission. *J. Phys. Chem. Lett.* 6, 5027–5033.
  32. Kulbak, M., Gupta, S., Kedem, N., Levine, I., Bendikov, T., Hodes, G., and Cahen, D. (2016). Cesium enhances long-term stability of lead bromide perovskite-based solar cells. *J. Phys. Chem. Lett.* 7, 167–172.
  33. Protesescu, L., Yakunin, S., Bodnarchuk, M.I., Krieg, F., Caputo, R., Hendon, C.H., Yang, R.X., Walsh, A., and Kovalenko, M.V. (2015). Nanocrystals of cesium lead halide perovskites ( $\text{CsPbX}_3$ , X = Cl, Br, and I): novel optoelectronic materials showing bright emission with wide color gamut. *Nano Lett.* 15, 3692–3696.
  34. Shang, Q., Li, M., Zhao, L., Chen, D., Zhang, S., Chen, S., Gao, P., Shen, C., Xing, J., Xing, G., et al. (2020). Role of the exciton-polariton in a continuous-wave optically pumped  $\text{CsPbBr}_3$  perovskite laser. *Nano Lett.* 20, 6636–6643.
  35. Fu, Y., Zhu, H., Stoumpos, C.C., Ding, Q., Wang, J., Kanatzidis, M.G., Zhu, X., and Jin, S. (2016). Broad wavelength tunable robust lasing from single-crystal nanowires of cesium lead halide perovskites ( $\text{CsPbX}_3$ , X = Cl, Br, I). *ACS Nano* 10, 7963–7972.
  36. Hu, Z., Liu, Z., Bian, Y., Liu, D., Tang, X., Hu, W., Zang, Z., Zhou, M., Sun, L., Tang, J., et al. (2017). Robust cesium lead halide perovskite microcubes for frequency upconversion lasing. *Adv. Opt. Mater.* 5, 1700419.
  37. Huang, C.Y., Zou, C., Mao, C., Corp, K.L., Yao, Y.C., Lee, Y.J., Schlenker, C.W., Jen, A.K.Y., and Lin, L.Y. (2017).  $\text{CsPbBr}_3$  perovskite quantum dot vertical cavity lasers with low threshold and high stability. *ACS Photon.* 4, 2281–2289.
  38. Wang, Y., Li, X., Nalla, V., Zeng, H., and Sun, H. (2017). Solution-processed low threshold vertical cavity surface emitting lasers from all-inorganic perovskite nanocrystals. *Adv. Funct. Mater.* 27, 1605088.
  39. Liu, Z., Yang, J., Du, J., Hu, Z., Shi, T., Zhang, Z., Liu, Y., Tang, X., Leng, Y., and Li, R. (2018). Robust subwavelength single-mode perovskite nanocuboid laser. *ACS Nano* 12, 5923–5931.
  40. Yang, Z., Lu, J., ZhuGe, M., Cheng, Y., Hu, J., Li, F., Qiao, S., Zhang, Y., Hu, G., Yang, Q., et al. (2019). Controllable growth of aligned monocrystalline  $\text{CsPbBr}_3$  microwire arrays for piezoelectric-induced dynamic modulation of single-mode lasing. *Adv. Mater.* 31, 1900647.
  41. Yan, D., Shi, T., Zang, Z., Zhao, S., Du, J., and Leng, Y. (2020). Stable and low-threshold whispering-gallery-mode lasing from modified  $\text{CsPbBr}_3$  perovskite quantum dots@ $\text{SiO}_2$  sphere. *Chem. Eng. J.* 401, 126066.
  42. Meyns, M., Perálvarez, M., Heuer-Jungemann, A., Hertog, W., Ibáñez, M., Nafria, R., Genç, A., Arbiol, J., Kovalenko, M.V., Carreras, J., et al. (2016). Polymer-enhanced stability of inorganic perovskite nanocrystals and their application in color conversion LEDs. *ACS Appl. Mater. Interfaces* 8, 19579–19586.
  43. De Giorgi, M.L., Krieg, F., Kovalenko, M.V., and Anni, M. (2019). Amplified spontaneous emission threshold reduction and operational stability improvement in  $\text{CsPbBr}_3$  nanocrystals films by hydrophobic functionalization of the substrate. *Sci. Rep.* 9, 17964.
  44. Liao, Q., Hu, K., Zhang, H.H., Wang, X.D., Yao, J.N., and Fu, H.B. (2015). Perovskite microdisk microlasers self-assembled from solution. *Adv. Mater.* 27, 3405–3410.